BULLETIN OF THE POLISH ACADEMY OF SCIENCES
TECHNICAL SCIENCES, Vol. 72(6), 2024, Article number: e151953
DOI: 10.24425/bpasts.2024.151953

MECHANICAL AND AERONAUTICAL ENGINEERING, THERMODYNAMICS

A sustainable approach-based optimization of internal diamond burnishing operation

An-Le VAN[1], Truong-An NGUYEN[2], Xuan-Ba DANG[3], and Trung-Thanh NGUYEN[2]*

[1] Faculty of Engineering and Technology, Nguyen Tat Thanh University, 300A Nguyen Tat Thanh, Ho Chi Minh City 700000, Vietnam
[2] Faculty of Mechanical Engineering, Le Quy Don Technical University, 236 Hoang Quoc Viet, Ha Noi 100000, Vietnam
[3] Department of Automatic Control, Ho Chi Minh City University of Technology and Education,
1 Vo Van Ngan Street, Linh Chieu Ward, Thu Duc City, Ho Chi Minh City 700000, Vietnam

Abstract. The related work of the diamond burnishing processes focused on improvements in surface quality. The study aims to optimize burnishing factors, including the spraying distance of the nozzle (S), the inlet pressure of the cold air (I), and the quantity of the liquid CO_2 (L) of the cool and cryogenic-assisted diamond burnishing operation for minimizing energy consumed (EC) and arithmetical mean surface height roughness (Sa). Burnishing responses are modelled based on the radial basis function network and full factorial data. The entropy method, improved grey wolf optimizer, non-dominated sorting genetic algorithm II, and technique for order of preference by similarity to the ideal solution were implemented to calculate the weights, produce solutions, and select the best outcome. As a result, the optimal data of the S, I, and L were 15.0 mm, 3.0 bar, and 11.0 L/min, respectively. The Sa and EC were reduced by 20.4% and 3.8%, respectively, at the optimality. The optimized outcomes could be employed to improve energy efficiency and machining quality for the internal diamond burnishing process. The optimizing technique could be used to solve complicated issues for different burnishing operations. The cool and cryogenic-assisted diamond burnishing process could be utilized for machining different internal holes.

Keywords: internal burnishing; cryogenic CO_2; energy consumed; surface roughness; optimization.

1. INTRODUCTION

The diamond burnishing process is renowned for its ability to produce a glossy surface finish with minimized friction. It offers additional benefits, such as a hardened surface layer for enhanced wear resistance and a compact surface topology that provides improved chemical resistance. The diamond tip smooths and polishes the surface when pressure is applied, reducing the need for additional finishing operations such as honing and polishing. Consequently, diamond burnishing operations can be considered a cost-effective method for machining ferrous and nonferrous materials.

Various burnishing processes have been considered and optimized to boost technical performances. A set of experiments on the burnished GCR15 steel was conducted to investigate the fatigue performance [1]. The authors indicated that the fatigue strength was increased by 36%, as compared to the unburnished case. The surface properties of the burnished butt joints of the 2024 aluminium alloy were investigated by Kluz *et al*. The results revealed that the surface roughness and Vickers hardness were enhanced by 73.8% and 84.2%, respectively, with the aid of the diamond burnishing operation [2]. The MQL-assisted burnishing operation was developed to facilitate the external surface [3]. The authors stated that the total carbon emission and the roughness of the external diamond burnishing operation were reduced by 3.8% and 11.6% with the aid of the Taguchi method. Sachin *et al.* demonstrated that the ideal spindle speed, feed rate, and burnishing force could be used to achieve the surface roughness of 0.2 µm and Vickers hardness of 397.5 HV for the cryogenic burnished 17-4 steel [4]. The impacts of the burnishing speed, feed, and force on the surface properties of 42CrMo4 hard-turned steel were explored [5]. The authors presented that the force was the most dominant factor, and the Vickers hardness was enhanced by 51.0%. A FEM model was developed to predict the roughness of the burnished surface [6]. The small errors between the simulated and actual data indicated the effectiveness of the proposed model. The Kriging models of the coefficient of friction, energy efficiency, and specific wear rate were developed in terms of the burnishing factors [7]. The authors stated that the responses were primarily affected by the burnishing speed and depth. Maximov *et al.* presented that the fatigue limit of the burnished 304 steel could be improved by 36.4%, as compared to untreated specimens [8]. A new burnishing tool was developed to enhance the wear corrosion of the burnished cylinder [9]. The authors presented that the wear rate of the specimen was reduced by 68.2%, as compared to the unburnished case. A multi-objective optimization was conducted using the desirability function for the sliding burnishing AISI 52100 steel [10]. The results revealed that the surface roughness and Vickers hardness were improved by 92% and 117%, respectively, while the fatigue life was increased up to 120%. A simulation model using the Cowper–Symonds coefficients was proposed to effectively predict the stress and deformation of the burnished 41Cr4 steel [11].

*e-mail: trungthanhnguyen@lqdtu.edu.vn

Manuscript submitted 2024-04-21, revised 2024-08-10, initially accepted for publication 2024-08-27, published in November 2024.

As a result, various diamond burnishing operations with MQL and cryogenic conditions were developed. However, a novel diamond burnishing process comprising the cryogenic CO_2 and Vortex tube was not developed. The proposed operation can be considered a sustainable burnishing process due to the elimination of any lubricants. The *EC* and *Sa* models regarding cooling parameters were not proposed for the internal diamond burnishing process. The optimal cooling parameters were not selected to reduce the *EC* and *Sa*. Moreover, the cool and cryogenic-assisted burnishing process of chromium-molybdenum steel (SCM440) was not proposed [12].

2. OPTIMIZATION APPROACH

In this work, the *EC* and *Sa* of the cool and cryogenic-assisted diamond burnishing operation are minimized by selecting optimal spraying distance, inlet pressure, and CO_2 quantity. The radial basis function network (RBFN) is used to develop the response models. The entropy method, improved grey wolf optimizer (IGWO), nondominated sorting genetic algorithm II (NSGA II), and technique for order of preference by similarity to ideal solution (TOPSIS) are employed to calculate the weights, produce solutions, and select the best outcome.

The *Sa* is computed as

$$Sa = \frac{\sum_{i=1}^{5} Sa_i}{5}, \tag{1}$$

where Sa_i is the arithmetical mean surface height roughness at the measured location.

The *EC* is computed as

$$EC = \sum_{i=1}^{10} P_{mi} \times t_m, \tag{2}$$

where P_{mi} and t_m are the power consumed at the i-th time and machining time, respectively.

The cooling parameters, including the S, I, and L are presented in Table 1. The ranges of each factor are determined based on the characteristics of the Vortex tube and CO_2 storage tank. Related works and burnishing experts confirm these values. The experimental values of the spindle speed, feed rate, and depth of penetration are 630 rpm, 0.05 mm/rev, and 0.06 mm, respectively.

Table 1
Diamond burnishing factors

Symbol	Cooling factors	Values
S	Spraying distance of the nozzle (mm)	15.0–25.0–35.0
I	Inlet pressure of the cold air (bar)	2.0–4.0–6.0
L	Quantity of the liquid CO_2 (L/min)	4.0–8.0–12.0

The optimizing approach is presented in Fig. 1:
Step 1: Performing burnishing experiments [13].
Step 2: Developing RBFN models for responses [14].

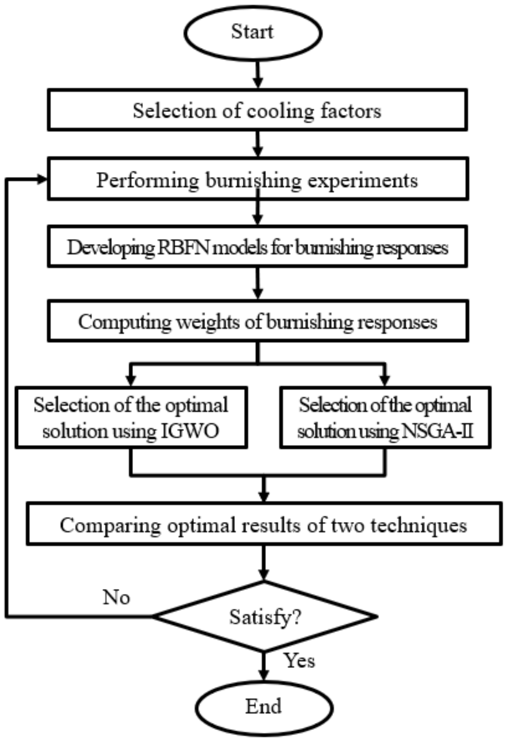

Fig. 1. Optimization approach

The RBFN is utilized to present experimental data with the aid of the Gaussian function. RBFN is a special type of feed-forward neural network with three layers, including the input, hidden layer, and output. The network receives an n-dimensional input vector, while the Euclidean distance between the input vector and each neuron centre is computed at the hidden layer. The output node is used to calculate a score based on a weighted sum of the activation values from the hidden layer and expressed as

$$\text{out}_i = \exp\left(-\frac{1}{2\sigma^2}\|s - c_i\|^2\right). \tag{3}$$

The Gaussian function is expressed as

$$\Phi(r) = \exp\left(-\gamma r^2\right), \tag{4}$$

where γ is a parameter, which is computed at the cross-validation stage.

The RBFN model for a given input is expressed as

$$\text{out} = w_0 + \sum_{i=1}^{m} w_i \exp\left(-\frac{1}{2\sigma^2}\|s - c_i\|^2\right), \tag{5}$$

where w_0 and $w_m$are the bias and weight, respectively.
Step 3: Computing the weight of each response.

The normalized response (n_{ij}) is computed as

$$n_{ij} = \frac{r_{ij}}{\sum_{i=1}^{m} r_{ij}}. \tag{6}$$

The entropy value (e_j) of each response is computed as

$$e_j = -\frac{\sum_{j=1}^{m} n_{ij} \times \ln n_{ij}}{\ln m}. \tag{7}$$

The weight (ω_i) is computed as

$$\omega_i = \frac{1-e_j}{\sum_{j=1}^{n}(1-e_j)}. \tag{8}$$

Step 4: Selection of the best optimal solution using the IGWO and TOPSIS.

In this work, the IGWO is proposed with the setting, evolution, and generation stages (Fig. 2).

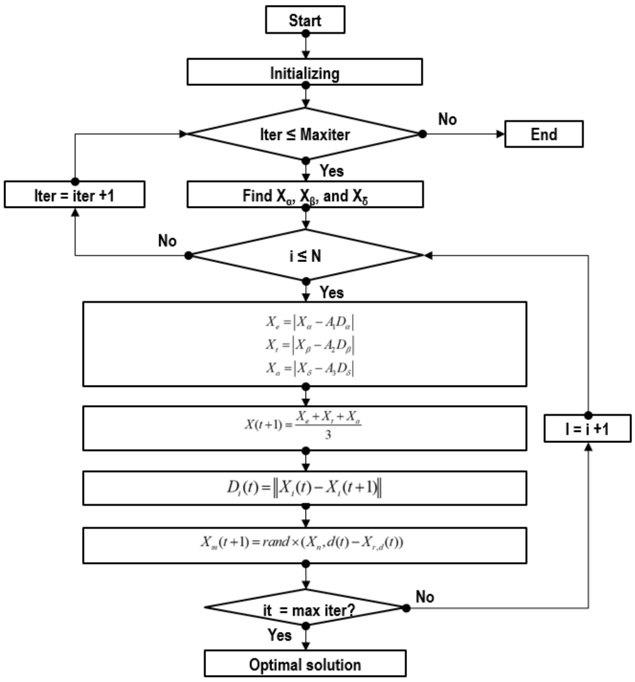

Fig. 2. The operating steps of the IGWO

In the setting stage, the wolves are distributed in the search space and expressed as

$$X_{ij} = l_j + \text{rand}_j \times (u_j - l_j), \tag{9}$$

where $X_i(t)$ is the position of the i-th wolf. l_j and u_j are the given ranges.

In the evolution stage, an individual is learned by their different neighbours. A radius $D_i(t)$ is calculated using Euclidean distance between the current position of $X_i(t)$ and the candidate position $X_i(t+1)$ and expressed as

$$D_i(t) = \|X_i(t) - X_i(t+1)\|. \tag{10}$$

The neighbour ($N_i(t)$) is expressed as

$$N_i(t) = \left\{X_j(t) \middle| D_i(X_i(t), X_j(t)) \le R_i(t)\right\}. \tag{11}$$

A prominent candidate $X_m(t+1)$ is expressed as

$$X_m(t+1) = \text{rand} \times \left(X_n, d(t) - X_{r,d}(t)\right), \tag{12}$$

where $X_{r,d}(t)$is a random wolf from the entire population.

The normalized solution (p_{ij}) is computed as [15]

$$p_{ij} = \frac{x_{ij}}{\sqrt{\sum_{i=1}^{m} x_{ij}}}. \tag{13}$$

A set of positive solution (S^+) is expressed as

$$S_i^+ = \sqrt{\sum_{j=1}^{m} \left(p_{ij} - p_j^+\right)^2}. \tag{14}$$

A set of positive solution (S^-) is expressed as

$$S_i^- = \sqrt{\sum_{j=1}^{m} \left(p_{ij} - p_j^-\right)^2}. \tag{15}$$

The evaluation indicator (E_I) is expressed as

$$E_I = \frac{S_i^-}{S_i^+ + S_i^-}. \tag{16}$$

3. EXPERIMENTAL FACILITIES

The burnishing trails are executed using a conventional lathe (Fig. 3). The 42CrMo4 steel is used to produce specimens due to its extensive usage in gears, engine shafts, and mould bushes. The length, internal diameter, and outer diameter of each specimen are 62 mm, 46 mm, and 56 mm, respectively. The drilling and internal turning operations are used to generate the hole. The cold air and cryogenic lubricant are produced from a Vortex tube and CO_2 tank, respectively. The burnishing device is clamped on the tool post. The burnishing length of 30 mm is conducted for all tests. The *Sa* of the initial surfaces is 4.632 µm. A new diamond tip is utilized after each burnishing trial.

The *Sa* values and power consumed are captured using the ZeGage Pro 3D optical profiler and Kyoritsu 6315 meter, respectively. The experimental results of No. 8 and 9 are depicted in Fig. 4.

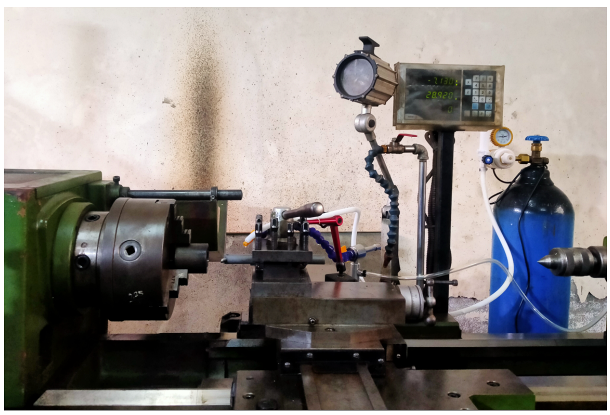

Fig. 3. Experiments of the diamond burnishing operation

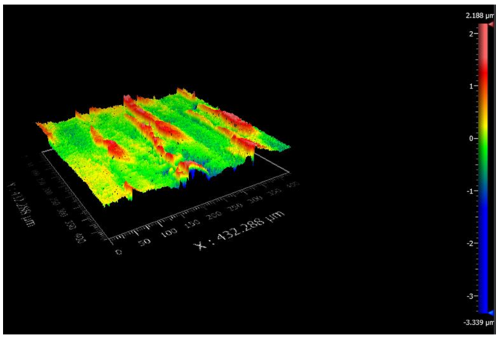

(a) *Sa* values at the experimental No. 8

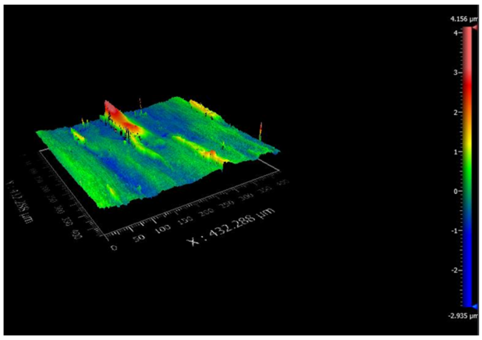

(b) *Sa* values at the experimental No. 9

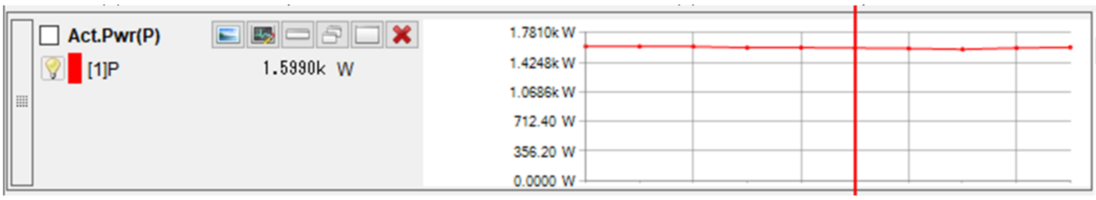

(c) The power consumed at the experimental No. 8

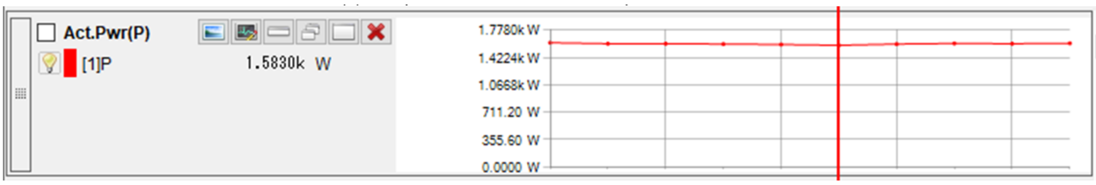

(d) The power consumed at the experimental No. 9

Fig. 4. Example results of the burnishing process

4. RESULTS AND DISCUSSIONS

The experimental results of the burnishing trials are exhibited in Table 2.

4.1. ANOVA analysis

The ANOVA results for the *Sa* model are shown in Table 3 [16–18]. The R^2 value of 0.9834 indicates that the developed model

Table 2
Experimental outcomes for the diamond burnishing operation

No.	*S* (mm)	*I* (bar)	*L* (L/min)	*Sa* (μm)	*EC* (kJ)	No.	*S* (mm)	*I* (bar)	*L* (L/min)	*Sa* (μm)	*EC* (kJ)	No.	*S* (mm)	*I* (bar)	*L* (L/min)	*Sa* (μm)	*EC* (kJ)
Data for developing RBFN models						Data for developing RBFN models						Data for testing the accuracy of RBFN models					
1	15.0	2.0	4.0	0.647	60.42	15	25.0	4.0	12.0	0.347	78.34	28	18.0	5.0	6.0	0.448	71.38
2	15.0	2.0	8.0	0.492	65.83	16	25.0	6.0	4.0	0.511	73.44	29	27.0	3.0	5.0	0.603	68.91
3	15.0	2.0	12.0	0.377	70.72	17	25.0	6.0	8.0	0.356	78.09	30	20.0	5.0	7.0	0.408	73.32
4	15.0	4.0	4.0	0.576	65.28	18	25.0	6.0	12.0	0.246	82.18	31	26.0	3.0	9.0	0.478	73.39
5	15.0	4.0	8.0	0.401	70.47	19	35.0	2.0	4.0	0.783	68.07	32	31.0	4.0	10.0	0.461	77.91
6	15.0	4.0	12.0	0.271	75.11	20	35.0	2.0	8.0	0.697	72.89	33	23.0	3.0	11.0	0.404	74.66
7	15.0	6.0	4.0	0.535	69.95	21	35.0	2.0	12.0	0.662	77.14	34	27.0	6.0	5.0	0.475	75.24
8	15.0	6.0	8.0	0.342	74.91	22	35.0	4.0	4.0	0.659	72.22	35	33.0	4.0	7.0	0.551	75.19
9	15.0	6.0	12.0	0.195	79.31	23	35.0	4.0	8.0	0.559	76.79	36	24.0	3.0	5.0	0.582	67.85
10	25.0	2.0	4.0	0.674	64.62	24	35.0	4.0	12.0	0.504	80.81	37	28.0	4.0	11.0	0.402	78.16
11	25.0	2.0	8.0	0.554	69.75	25	35.0	6.0	4.0	0.567	76.15	38	29.0	5.0	9.0	0.401	78.28
12	25.0	2.0	12.0	0.479	74.31	26	35.0	6.0	8.0	0.454	80.49	39	32.0	6.0	10.0	0.366	81.86
13	25.0	4.0	4.0	0.577	69.13	27	35.0	6.0	12.0	0.377	84.27	40	24.0	4.0	7.0	0.464	72.52
14	25.0	4.0	8.0	0.441	74.02												

Table 3
ANOVA results for the *Sa* model

So.	SS	MS	F-Value	p-value	Cont. (%)
Model	0.2459	0.0273	46.08	< 0.0001	
S	0.0500	0.1513	252.17	< 0.0001	17.52
I	0.0780	0.1881	313.49	< 0.0001	21.78
L	0.1100	0.2203	367.18	< 0.0001	25.51
SI	0.0025	0.0479	79.88	0.0007	5.55
SL	0.0056	0.0719	119.90	0.0005	8.33
IL	0.0012	0.0336	55.99	0.0009	3.89
S^2	0.0067	0.0767	127.81	0.0006	8.88
I^2	0.0009	0.0288	47.93	0.0009	3.33
L^2	0.0021	0.0450	74.99	0.0007	5.21
Residual	0.0041	0.0006			
Cor Total	0.25				
$R^2 = 0.9834$; Adjusted $R^2 = 0.9753$; Predicted $R^2 = 0.9678$					

is significant. As a result, the contributions of the S, I, and L are 17.52%, 21.78%, and 25.51%, respectively (Fig. 5a). The contributions of the SI, SL, and IL are 5.55%, 8.33%, and 3.89%, respectively. The contributions of the S^2, I^2, and L^2 are 8.88%, 3.33%, and 5.21%, respectively.

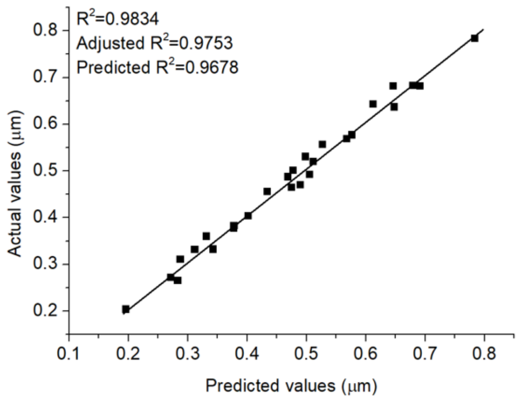

(a) For the *Sa* model

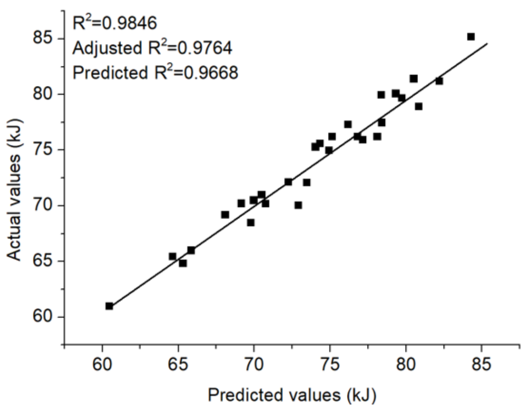

(b) For the *EC* model

Fig. 5. Comparisons between the predictive and actual values

The ANOVA results for the *EC* model are shown in Table 4. The R^2 value of 0.9846 indicates that the developed model is significant. As a result, the contributions of the S, I, and L are 23.19%, 30.63%, and 33.81%, respectively (Fig. 5b). The contributions of the SI, SL, and IL are 2.71%, 2.27%, and 1.77%, respectively. The contributions of the S^2 and L^2 are 2.83% and 2.05%, respectively.

Table 4
ANOVA results for the *EC* model

So.	SS	MS	F-Value	p-value	Cont. (%)
Model	385.29	42.81	36.82	< 0.0001	
S	79.86	1230.16	1430.42	< 0.0001	23.19
I	139.17	1624.83	1889.33	< 0.0001	30.63
L	169.67	1793.52	2085.49	< 0.0001	33.81
SI	0.54	143.76	167.16	0.0004	2.71
SL	0.38	120.42	140.02	0.0005	2.27
IL	0.23	93.89	109.18	0.0008	1.77
S^2	0.63	150.12	174.56	0.0003	2.83
I^2	0.04	39.25	45.65	0.8427	0.74
L^2	0.33	108.75	126.45	0.0006	2.05
Residual	6.03	0.86			
Cor Total	391.32				
$R^2 = 0.9846$; Adjusted $R^2 = 0.9764$; Predicted $R^2 = 0.9668$					

As shown in Figs. 6a and 6b, the data are distributed on straight lines; hence, the developed RBFN models are adequate. Table 5 presents the comparisons between the actual and RBFN-predicted outcomes. The slight variations (less than 5%) demonstrated that the RBFN models could be used to accurately predict burnishing responses.

Table 5
Testing results for developed RBFN models

No.	*Sa* (µm)			*EC* (KJ)		
	Exp.	RBFN	Er. (%)	Exp.	RBFN	Er. (%)
28	0.448	0.452	–0.89	71.38	70.92	0.64
29	0.603	0.598	0.83	68.91	69.34	–0.62
30	0.408	0.411	–0.74	73.32	73.86	–0.74
31	0.478	0.473	1.05	73.39	72.98	0.56
32	0.461	0.465	–0.87	77.91	78.24	–0.42
33	0.404	0.408	–0.99	74.66	74.28	0.51
34	0.475	0.471	0.84	75.24	75.48	–0.32
35	0.551	0.554	–0.54	75.19	74.98	0.28
36	0.582	0.586	–0.69	67.85	67.24	0.90
37	0.402	0.405	–0.75	78.16	78.35	–0.24
38	0.401	0.397	1.00	78.28	78.64	–0.46
39	0.366	0.363	0.82	81.86	81.36	0.61
40	0.464	0.468	–0.86	72.52	72.24	0.39

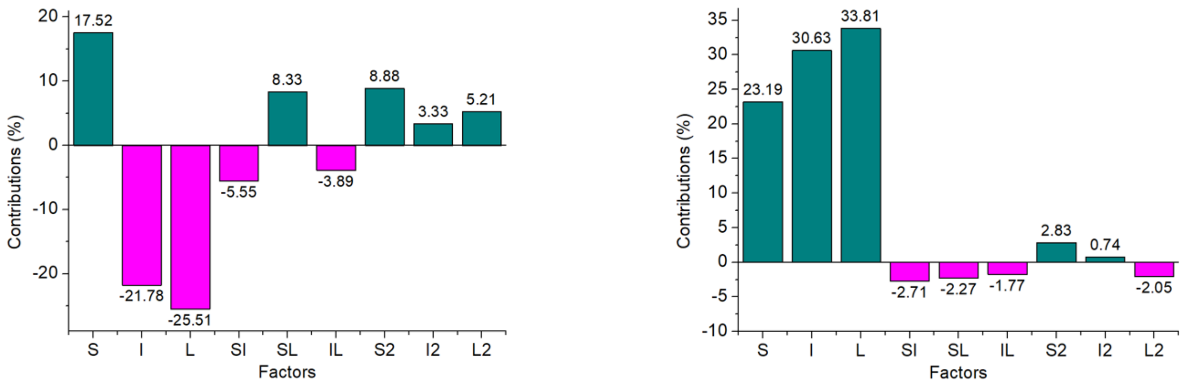

(a) Parametric contributions for the *Sa* model (b) Parametric contributions for the *EC* model

Fig. 6. Parametric contributions for burnishing responses

4.2. Parametric impacts

As a result, a higher inlet pressure causes a reduction in the roughness (Fig. 7a). At a low inlet pressure, the temperature of the cold air slightly reduces, resulting in a reduction in the cooling impact. This leads to a higher friction in the burnishing region; hence, the roughness increases. At a high inlet pressure, the temperature of the cold air significantly reduces, leading to lower friction in the burnishing region; hence, a lower roughness is obtained [19].

As a result, a higher CO_2 quantity causes a reduction in the roughness (Fig. 7b). At a high CO_2 quantity, an increased amount of liquid CO_2 is transferred into the interfaces, leading to low friction [19]. The material compression is easily performed; hence, the roughness is reduced.

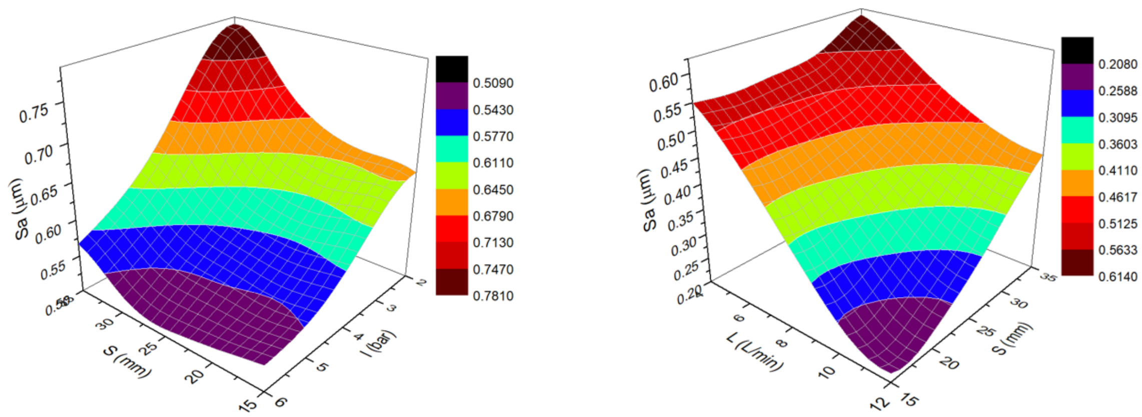

(a) *Sa* versus *S* and *I* (b) *Sa* versus *S* and *L*

Fig. 7. The main impacts of process parameters on the *Sa*

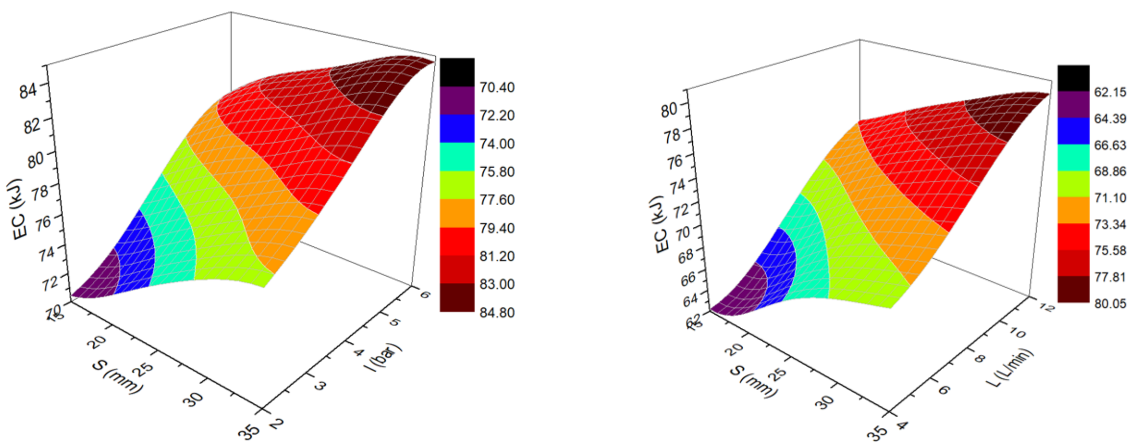

(a) *EC* versus *S* and *I* (b) *EC* versus *S* and *L*

Fig. 8. The main impacts of process parameters on the *EC*

As a result, more energy is consumed with a higher spraying distance (Fig. 8a). At a higher distance between the nozzle and specimen, increased friction is produced due to the low cooling impact [19]. An increase in energy is required to overcome a higher resistance. More energy is consumed with a higher inlet pressure (Fig. 8a). At a higher inlet pressure, cooler air is transferred into the interfaces, leading to higher specimen hardness [20]. An increase in energy is required to process the material.

As a result, more energy is consumed with a higher CO_2 quantity (Fig. 8b). A higher quantity of liquid CO_2 increases the workpiece hardness due to an efficient cooling impact [21]. A higher amount of energy is consumed to compress the specimen.

4.3. The optimal results

The computed weights of the *Sa* and *EC* are 0.63, and 0.37, respectively. Figure 9 shows the Pareto graphs produced by IGWO. As a result, a low energy has corresponded with a higher roughness. The best solution is selected using the TOPSIS. As a result, the optimal *S*, *I*, and *L* are 15.0 mm, 3.0 bar, and 11.0 L/min, respectively. At the selected solution, the *Sa* and *EC* are reduced by 20.4% and 3.8%, respectively (Table 6).

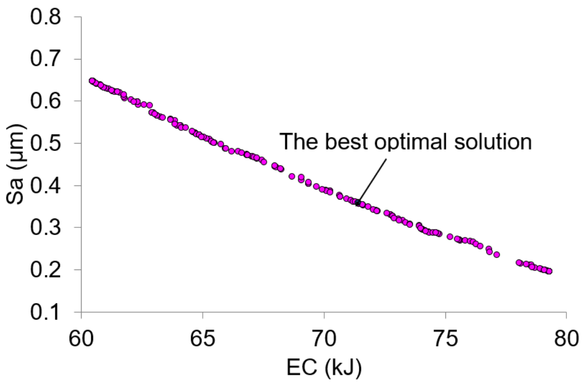

Fig. 9. Pareto fronts produced by the IGWO

The NSGA-II and TOPSIS are utilized to find optimal factors. As a result, the optimal *S*, *I*, and *L* are 15.0 mm, 2.0 bar, and 12.0 L/min, respectively (Table 6). The *Sa* and *EC* are reduced by 13.3% and 2.9%, respectively. It was pointed out that the IQWO provided better optimal results, as compared to the NSGA-II.

Table 6
Optimization results produced by the IGWO and NSGA-II

Method	*S* (mm)	*I* (bar)	*L* (L/min)	*Sa* (μm)	*EC* (kJ)	E_I
Initial results	25.0	4.0	8.0	0.441	74.02	
IQWO	15.0	3.0	11.0	0.351	71.22	0.884
Reductions by the IQWO (%)				–20.4	–3.8	
NSGA-II	15.0	2.0	12.0	0.382	71.86	0.832
Reductions by the NSGA-II (%)				–13.3	–2.9	

5. CONCLUSIONS

In this investigation, a cool and cryogenic-assisted diamond burnishing operation was developed and optimized. The reductions in the roughness and energy consumption were obtained using optimal *S*, *I*, and *L*. The RBFN, IGWO, NSGA-II, and TOPSIS were utilized to propose burnishing responses and select the optimality. The conclusions can be as follows:

1. A lower spraying distance could be used to minimize the *Sa* and *EC*. Higher inlet pressure, and CO_2 quantity could be applied to reduce the *Sa*. The lower inlet pressure and CO_2 quantity could be applied to save *EC*.
2. In terms of the *Sa* and *EC* models, the CO_2 quantity had the highest contribution, followed by the inlet pressure and spraying distance, respectively.
3. The optimal *S*, *I*, and *L* generated by the IGWO were 15.0 mm, 3.0 bar, and 11.0 L/min, respectively. The reductions in the *Sa* and *EC* were 20.4% and 3.8%, respectively.
4. The optimization approach can be effectively used to solve optimization issues for different burnishing processes.
5. The BRFN approach can be employed to present nonlinear relations of experimental data.
6. The developed cooling system can be effectively employed to facilitate other burnishing operations without any lubricants.
7. The developed burnishing operation can be utilized to produce surface finishing for interior holes.
8. The designed and fabricated tool can be utilized in other internal diamond burnishing operations.
9. To improve the roughness and energy efficiency of the practical diamond burnishing operation, optimal parameters and responses can be utilized.
10. The investigation results can be used to create an intelligent system that will enable the internal diamond burnishing operation across a range of industries.
11. The impacts of the process parameters on the hardness and the depth of the affected layer will be explored in future works.

REFERENCES

[1] O. Taamallah, H. Hamadache, N. Mokas, A. Amirat, and B. Hamadi, "Investigation of the effects of slide diamond burnishing process on the mechanical performance of GCr15 steel," *J. Fail. Anal. and Preven.*, vol. 23, pp. 1101–1113, 2023, doi: 10.1007/s11668-023-01652-5.

[2] R. Kluz, M. Bucior, A. Dzierwa, K. Antosz, W. Bochnowski, and K. Ochał, "Effect of diamond burnishing on the properties of FSW joints of EN AW-2024 aluminum alloys," *Appl. Sci.*, vol. 13, no. 2, p. 1305, 2023, doi: 10.3390/app13031305.

[3] T.T. Nguyen and A.L. Van, "Machining and optimization of the external diamond burnishing operation," *Mater. Manuf. Process.*, vol. 38, no. 10, pp. 1276–1290, 2023, doi: 10.1080/10426914.2022.2072880.

[4] B. Sachin, S. Narendranath, and D. Chakradhar, "Application of desirability approach to optimize the control factors in cryogenic

diamond burnishing," *Arab. J. Sci. Eng.*, vol. 45, pp. 1305–1317, 2020, doi: 10.1007/s13369-019-04326-3.

[5] J. Zaghal, V. Molnar, and M. Benke, "Improving surface integrity by optimizing slide diamond burnishing parameters after hard turning of 42CrMo4 steel," *Int. J. Adv. Manuf. Technol.*, vol. 128, pp. 2087–2103, 2023, doi: 10.1007/s00170-023-12008-6.

[6] C. Felhő and G. Varga, "CAD and FEM modelling of theoretical roughness in diamond burnishing," *Int. J. Precis. Eng. Manuf.*, vol. 23, pp. 375–384, 2022, doi: 10.1007/s12541-022-00622-5.

[7] T.T. Nguyen, T.A. Nguyen, A.L. Van, and X.B. Dang, "Multi-performance optimization of the diamond burnishing process in terms of energy saving and tribological factors," *Proc. Inst. Mech. Eng. E – J. Process Mech. Eng.*, 2023. doi: 10.1177/09544089231163407.

[8] J. Maximov, G. Duncheva, A. Anchev, V. Dunchev, and Y. Argirov, "Improvement in fatigue strength of chromium–nickel austenitic stainless steels via diamond burnishing and subsequent low-temperature gas nitriding," *Appl. Sci.*, vol. 14, no. 3, p. 1020, 2024, doi: 10.3390/app14031020.

[9] G.V. Duncheva, J.T. Maximov, A. Anchev, V. Dunchev, Y. Argirov, and S. Velkov, "Modeling and optimization of surface integrity and sliding wear resistance of diamond-burnished holes in austenitic stainless steel cylinder lines," *Machines*, vol. 11, p. 872, 2023, doi: 10.3390/machines11090872.

[10] T. Ouahiba, H. Hamid, B. Selma, and L. Laouar, "Multi-objective optimization of slide diamond burnishing parameters for enhanced fatigue resistance of AISI 52100 steel," *J. Braz. Soc. Mech. Sci. Eng.*, vol. 46, p. 451, 2024, doi: 10.1007/s40430-024-05001-x.

[11] J.T. Maximov and G.V. Duncheva, "Effects of cryogenic- and cool-assisted burnishing on the surface integrity and operating behavior of metal components: A review and perspectives',' *Machines*, vol. 12, p. 312, 2024; doi: 10.3390/machines12050312.

[12] J. Chodór *et al.*, "Using the FEM method in the prediction of stress and deformation in the processing zone of an elastic/visco-plastic material during diamond sliding burnishing," *Appl. Sci.*, vol. 13, no. 3, p. 1963, 2023, doi: 0.3390/app13031963.

[13] S.C. Cagan, M. Maci, M.M. Buldum, and C. Maci, "Artificial neural networks in mechanical surface enhancement technique for the prediction of surface roughness and microhardness of magnesium alloy," *Bull. Polish Acad. Sci. Tech. Sci.*, vol. 67, pp. 729–739, 2019, doi: 10.24425/bpasts.2019.130182.

[14] P. Zhou and M. Tan, "Robust zeroing neural networks with two novel power-versatile activation functions for solving dynamic Sylvester equation," *Bull. Pol. Acad. Sci. Tech. Sci.*, vol. 70, p. e141307, 2022, doi: 10.24425/bpasts.2022.141307.

[15] Q. Chenghui, W. Chongtian, Y. Xiaolu, W. Linxu, Y. Jiaming, and S. Hong, "Multi-objective optimization of PCM-fin structure for staggered Li-ion battery packs," textitBull. Pol. Acad. Sci. Tech. Sci., vol. 71, no. 4, p. e145677, 2023, doi: 10.24425/bpasts.2023.145677.

[16] A. Saldaña-Robles, H. Plascencia-Mora, E. Aguilera-Gómez, A. Saldaña-Robles, A. Marquez-Herrera, and J.A. Diosdado-De la Peña, "Influence of ball-burnishing on roughness, hardness and corrosion resistance of AISI 1045 steel," *Surf. Coat. Technol.*, vol. 339, pp. 191–198, 2018, doi: 10.1016/j.surfcoat.2018.02.013.

[17] B. Buldum and S. Cagan, "Study of ball burnishing process on the surface roughness and microhardness of AZ91D Alloy," *Exp. Tech.*, vol. 42, pp. 233–241, 2018, doi: 10.1007/s40799-017-0228-8.

[18] G.D. Revankar, R. Shetty, S.S. Rao, and V.N. Gaitonde, "Analysis of surface roughness and hardness in ball burnishing of titanium alloy," *Measurement*, vol. 58, pp. 256–268, 2014, doi: 10.1016/j.measurement.2014.08.043.

[19] M.T. Le, A.L. Van, T.T. Nguyen, and X.B. Dang, "Ecological design optimization of nozzle parameters for burnishing operation," *J. Appl. Eng. Sci.*, vol. 21, no. 2, pp. 686–697, 2023, doi: 10.5937/jaes0-41943.

[20] T.T. Nguyen, T.A. Nguyen, Q.H. Trinh, and X.B. Le, "Multi-performance optimization of multi-roller burnishing process in sustainable lubrication condition," *Mater. Manuf. Process.*, vol. 37, no. 4, pp. 407–427, 2021, doi: 10.1080/10426914.2021.1962533.

[21] B. Huang, Y. Kaynak, Y. Sun, and I.S. Jawahir, "Surface Layer modification by cryogenic burnishing of Al 7050-T7451 alloy and validation with FEM-based burnishing model," *Procedia CIRP*, vol. 31, pp. 1–6, 2015, doi: 10.1016/j.procir.2015.03.097.